energy&fuels

Article

pubs.acs.org/EF

Nanoaggregates of Diverse Asphaltenes by Mass Spectrometry and Molecular Dynamics

Weiguo Wang,[†,¶] Cooper Taylor,[§] Hui Hu,[§] Kathryn L. Humphries,[∥] Arjun Jaini,[§] Michael Kitimet,[§] Thais Scott,[§] Zach Stewart,[§] Kevin John Ulep,[§] Shannon Houck,[§] Adam Luxon,[§] Boyi Zhang,[§] Bill Miller,[∥] Carol A. Parish,[§] Andrew E. Pomerantz,[⊥] Oliver C. Mullins,*[,⊥] and Richard N. Zare[†]

[†]Department of Chemistry, Stanford University, Stanford, California 94305, United States

[§]Department of Chemistry, Gottwald Center for the Sciences, University of Richmond, Richmond, Virginia 23173, United States

[∥]Department of Chemistry, Truman State University, Kirksville, Missouri 63501, United States

[⊥]Schlumberger-Doll Research, Cambridge, Massachusetts 02139, United States

ABSTRACT: Asphaltene nanoaggregates from three diverse source materials—coal-derived asphaltenes dominated by aromatic carbon, petroleum asphaltenes with comparable abundances of aromatic and aliphatic carbon, and immature source-rock asphaltenes dominated by aliphatic carbon—are examined by means of surface-assisted laser desorption ionization mass spectrometry (SALDI-MS) coupled with laser desorption laser ionization mass spectrometry (L^2MS). All three types of asphaltenes form nanoaggregates with aggregation numbers close to 7. Molecular dynamics calculations for proposed island molecular structures show the important roles that π-stacking and alkane steric hindrance play in nanoaggregate formation and structure. These results are discussed in terms of entropy and enthalpy changes. All results are consistent with the Yen-Mullins model, which bodes well for its expanded use in oilfield reservoir evaluations.

INTRODUCTION

Asphaltenes are defined as the fraction of a carbonaceous mixture (such as petroleum) that dissolves in aromatic solvent (such as toluene) but precipitates in aliphatic solvent (such as *n*-heptane). Petroleum asphaltenes play a key role in many aspects of oil production and refining, and as a result they have been the subject of numerous investigations.[1−3] The solubility classification of asphaltenes (*n*-heptane insoluble, toluene soluble) suggests that different asphaltenes could have similar aggregation properties. Petroleum asphaltene aggregation has numerous industrial consequences related to phase behavior and flow assurance,[4] coking in refining, tar mat deposition in reservoirs,[5−7] and fluid gradients in reservoirs.[8−13] Thus, characterization of asphaltenes has focused on both their molecular structure and their aggregate structure.

Dominance of Island Architecture for Asphaltenes. For the modeling undertaken in this work, the molecular architecture of asphaltenes is key. A review of many studies indicates that asphaltenes are overwhelmingly dominated by island molecular architecture with a single PAH in the molecule. Here, we discuss the large number of studies which establish molecular weight of asphaltenes and the dominance of island architecture. Petroleum asphaltenes have molecular weights typically in the range 500−1000 Da. The molecular weights are supported by various experimental techniques such as molecular diffusion methods using time-resolved fluorescence depolarization,[14−16] fluorescence correlation spectroscopy,[17,18] Taylor dispersion,[19] and NMR diffusion measurements.[20] Naturally, mass spectroscopy has also been critical in molecular weight determination of asphaltenes including laser desorption ionization mass spectrometry (LDI MS),[21] laser-induced acoustic desorption mass spectrometry (LIAD MS),[22] two-step laser desorption laser ionization mass spectrometry (L^2MS),[23−25] and electrospray ionization, Fourier-transform ion cyclotron resonance mass spectrometry (ESI-FT-ICR-MS).[26] Particularly relevant is L^2MS, in which asphaltenes are volatilized by an infrared laser, ionized by an ultraviolet laser, and finally detected by a time-of-flight mass analyzer. In L^2MS, the volatilization process involves extremely rapid heating (10^8 °C/s), which suppresses fragmentation. The ionization process involves nonresonant single photon absorption, which is approximately equally efficient for a wide range of molecular classes. A delay between volatilization and ionization laser pulses prevents ion-induced dipole attraction (due to plume expansion), suppressing aggregation; and the use of time-of-flight detection without reflection further provides approximately equally efficient detection across a wide range of molecular weights. As a result, the L^2MS method has been thoroughly investigated and found to detect asphaltenes with minimal fragmentation, negligible aggregation, and nearly invariant detection cross section for different molecular structures in asphaltenes, ruling out significant bias in the results.[27,28]

The island architecture or single aromatic core geometry is supported by various experimental techniques including time-resolved fluorescence depolarization measurements (TRFD) demonstrating a strong correlation between rotational diffusion time and fused ring size.[14−16] While these experiments were the first to show a single core, they are limited to molecules that fluoresce. These TRFD results of a single aromatic core were

Received: May 16, 2017
Revised: August 3, 2017
Published: August 4, 2017

DOI: 10.1021/acs.energyfuels.7b01420
Energy Fuels 2017, 31, 9140−9151

subsequently supported by L^2MS measurements that are known to access virtually the entire molecular population of asphaltenes. These L^2MS studies showed that under higher laser power, all (>10) archipelago model compounds investigated underwent unimolecular decomposition while all (>10) island model compounds investigated and asphaltenes did not undergo decomposition.[25] L^2MS capabilities specifically for asphaltenes and related compounds are treated at length in Experimental Methods. Other mass spectroscopy studies also support the dominance of island architecture. Fragmentation of asphaltenes and model compounds by different means supported the island architecture.[29] A study examining 6 different asphaltenes by collisionally activated dissociation in tandem mass spectrometry concluded in the abstract, "The results obtained support the island structural model for these asphaltenes".[30] Interfacial studies on asphaltenes and model compounds determined the molecular contact area and also support island architecture.[31] These studies are consistent with the direct determination of the orientation of asphaltene molecules at the oil−water interface.[32]

Recently, workers at IBM Zurich and colleagues used ultrahigh resolution molecular imaging by atomic force microscopy (AFM) and scanning tunneling microscopy (STM) and confirmed the dominance of island molecular architecture of asphaltenes.[33,34] A very diverse set of asphaltenes was obtained from workers at Schlumberger, ExxonMobil, Shell, and Chevron with hundreds of images;[34] not even one traditional archipelago molecule (with PAHs linked by an alkane bridge) was found. Moreover, exactly the same imaging methods were shown to easily image a large variety of traditional archipelago model compounds synthesized in the laboratory.[35] The conclusion is reached that traditional archipelago compounds are not obtained in the imaging studies of asphaltenes because they are not present in any significant fraction in asphaltenes.[33,34] Perhaps the instability of traditional archipelago molecules suggested by unimolecular decomposition studies is why such molecules are not found in asphaltenes.[25]

Some previous studies based on techniques such as bulk decomposition suggested a dominance of structures with multiple aromatic cores.[36] However, it is known that bulk decomposition methods used in these studies lead to synthesis of archipelago compounds from island model compounds as stated in the title of the paper.[37] With such a conversion of island models to archipelago structures in bulk decomposition studies, it is evident that such methods are not reliable to determine virgin molecular architectures. Moreover, it is important to prove that reactive chemistry is not altering the sample in any corresponding method used to identify molecular architecture.

Aggregation of Asphaltenes. On an aggregate level, asphaltenes are described by a hierarchical aggregation codified in the Yen-Mullins model.[2,3] As described by this model, at concentrations exceeding the critical nanoaggregate concentration (CNAC), asphaltenes form nanoaggregate structures consisting of 5−10 molecules; at concentrations exceeding the critical cluster concentration (CCC), asphaltenes form clusters consisting of 5−10 nanoaggregates; and at yet higher concentrations, asphaltenes can form larger aggregate structures leading to flocculation. A variety of studies have shown that the CNAC occurs at concentrations of $\sim 10^{-4}$ mass fraction (or $\sim 10^{-4}$ molar).[20,38−42] These and other studies also support the estimation of the size of the nanoaggregate at approximately 5−10 molecular sizes.[43] Additionally, asphaltene nanoaggregate sizes have been measured by surface assisted laser desorption ionization (SALDI) mass spectrometry. In SALDI, asphaltenes are simultaneously volatilized from a surface and ionized by a single ultraviolet laser pulse, prior to detection with a time-of-flight mass analyzer.[28,44] Unlike L^2MS, in SALDI the volatilization and ionization processes are not separated in space or in time, so aggregation is not suppressed. If relatively low laser power is employed, asphaltenes will be detected by SALDI as nanoaggregates. Using SALDI, asphaltene nanoaggregate masses equal to 5−10 molecular masses have been measured.[44]

The structures of asphaltene nanoaggregates have been studied experimentally and theoretically. Studies combining small angle neutron scattering (SANS) and small-angle X-ray scattering (SAXS) determined that asphaltene nanoaggregates have a core of aromatic carbon surrounded by a periphery of saturate carbon.[45] Aggregation has been attributed to π-stacking interactions between the aromatic cores of asphaltenes.[38,46,47] This interaction is driven by the polarizability of the aromatic cores, but alkane substitution can interfere with ordered PAH stacking. Heteroatoms incorporated into the asphaltenes are believed to play a secondary role.[46,47] Asphaltenes are sufficiently polydisperse that long-range order is precluded, and small aggregation numbers have been predicted.[2,3,48]

Although much work has focused on analysis of asphaltenes derived from petroleum, asphaltenes can be derived from other sources. Asphaltenes derived from different sources share the same solubility characteristics by definition (e.g., toluene soluble, *n*-heptane insoluble), but the composition of asphaltenes derived from different sources can vary greatly. For example, a key chemical parameter that can differ is the aromaticity (measured by ^{13}C NMR), which for carbonaceous materials correlates strongly with the ratio of hydrogen to carbon.[49] Virgin petroleum asphaltenes (PAs), that is, petroleum asphaltenes that have not been subjected to any processing such as refining, have an aromaticity near 50% and an H:C ratio of ∼1.1.[2,50] Coal-derived asphaltenes (CDAs) have much less alkane carbon in line with the source material. Coal originates from terrestrial plants, enriched in the aromatic lignins, and is deposited in a more oxic environment compared to petroleum source materials, thereby reducing hydrogen content. Coal-derived asphaltenes are obtained from the process of hydrogenation creating coal liquids which are then refined. CDAs are then obtained from the corresponding vacuum resid.[16,51] CDAs have an aromaticity near 80% and an H:C ratio of ∼0.8.[50] In contrast, immature source rock asphaltenes (ISAs) are enriched in alkane carbon, thus in hydrogen; immature source rock has not experienced significant catagenesis, a process that results in cleavage of alkane substituents generating oil.[52] Consequently, the asphaltenes from immature source rock have an aromaticity near 30% and an H:C ratio of ∼1.4.[53]

Analyzing asphaltenes from different sources, which have diverse chemical compositions but identical solubilities (in toluene and heptane), helps to elucidate how chemical structure impacts the aggregation process. In this paper, the aggregation numbers (number of asphaltene molecules per nanoaggregate) of PAs, CDAs, and ISAs are determined by L^2MS measurement of molecular weight and SALDI measurement of nanoaggregate weight. Structures representative of these three asphaltene types are modeled, and the aggregation of those models is probed by molecular dynamics simulation.

DOI: 10.1021/acs.energyfuels.7b01420
Energy Fuels 2017, 31, 9140−9151

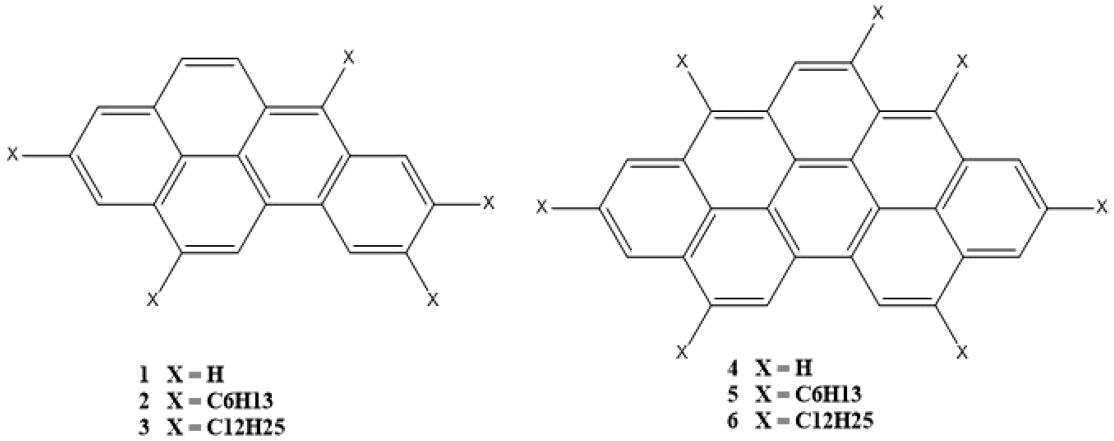

Figure 1. Initial asphaltene model compounds. **1** and **4** probed aromatic effects while **2,3** and **5,6** probed the effects of alkylation.

Modeling was performed in the gas phase to understand the underlying structure−function relationship between various types of asphaltenes as well as to provide an atomistic interpretation of the gas-phase experimental work. The structure of the nanoaggregates as a function of alkane carbon is of particular interest. We are interested in the interactions that are possible between asphaltene molecules and this will provide a rigorous baseline with which to interpret future solvent-phase studies. The results provide insight into the relationship between molecular structure and nanoaggregate structure as well as the role of entropy and enthalpy in nanoaggregate formation.

EXPERIMENTAL METHODS

Sample Preparation. Two petroleum asphaltenes (PA) from Kuwait, UG8 and BG5, have been examined. These petroleum asphaltenes were extracted from crude oils by diluting the crude oil 1:40 in *n*-heptane and stirring for 24 h. Asphaltenes were extracted from the solution by filtration through a nylon membrane with 0.65 μm pores. The samples were washed with additional *n*-heptane until the wash solvent was colorless. Finally, the asphaltenes were washed by Soxhlet extraction in *n*-heptane for 2 days.

Coal-derived asphaltenes (CDA) from Adaro coal have been described before.[51] The coals were liquefied and distilled, and the distillation residue was then extracted to obtain coal-derived asphaltenes. The typical liquefaction conditions were at a temperature of 450−465 °C, a pressure of 16.8 MPa (in part from added H_2), with a gas/feed slurry ratio of 0.7 N m3/kg, and a coal concentration in the feed slurry of 40 wt %. The distillation residue was the fraction boiling above 538 °C. The asphaltene fraction, which is toluene soluble and *n*-hexane-insoluble, was obtained by Soxhlet extraction of the distillation residue. The Wyoming coal CDA was obtained by a similar liquefaction and distillation process; this is also a residual asphaltene.[54]

Immature source rock asphaltene (ISA) was extracted from an unweathered outcrop from an immature section of the Eagle Ford.[55] The bitumen fraction of that rock was isolated by Soxhlet extraction in 90:10 dichloromethane:methanol. The asphaltene fraction of the bitumen was then isolated from the bitumen using the same procedure as described above for isolating the PAs from crude oil. The ISAs were then dissolved in toluene to ensure they meet the solubility definition of asphaltenes. It was observed that the entire asphaltene fraction, originally dissolved in 90:10 dichloromethane:methanol, is toluene soluble.

Mass Spectrometry. The asphaltene samples were analyzed by L^2MS and SALDI mass spectrometry at Stanford University. The L^2MS method of measuring asphaltene molecular weight has been described in detail previously.[23−25,27,44,56−61] Many methods are available to measure the molecular weight of asphaltenes, each with its own advantages and limitations. L^2MS is perhaps the most thoroughly investigated method of asphaltene molecular weight analysis, and it has been found that the main advantage of L^2MS is an essentially unbiased detection of nearly all of the components in asphaltenes (with minimal fragmentation, minimal aggregation, and nearly identical detection sensitivities across the different classes of compounds potentially occurring in asphaltenes) while the main limitation is modest mass resolution and accuracy (with typical uncertainty nearly 1 Da, preventing assignment of molecular formulas from L^2MS measurements).[23−25,27,44,56,57,59−61] The nearly unbiased detection in L^2MS originates from many factors, each of which are expected mechanistically and demonstrated experimentally. Ionization in L^2MS occurs via single photon ionization,[62] with the photon energy just above the typical ionization potential. As a result, little energy is left over after ionization, insufficient to cause fragmentation. Additionally, volatilization is achieved by laser desorption at rapid heating rates (nearly 10^8 K/s),[63] further suppressing fragmentation. Experimentally, analysis of dozens of model compounds of widely ranging structure found little fragmentation, with the largest signal consistently coming from the parent ion.[27,28,56,57] Ionization in L^2MS occurs after the desorbed plume of neutrals has dispersed into the vacuum. As a result, the molecules are too far apart by the time they are ionized to be bound together by ion-induced dipole attraction, preventing aggregation. Experimentally, analysis of the same set of model compounds does not result in measurable signal from any aggregate.[27,28,56,57] Similar detection sensitivities result from the methods used for volatilization (nonselective laser desorption, in which the entire asphaltene sample is desorbed in the area struck by the laser pulse),[28] ionization (single photon ionization, which is a universal soft ionization method for compounds with ionization potential below the photon energy),[62] and mass analysis (by time-of-flight, which detects components with nearly equal sensitivity over a large, theoretically unlimited, mass range).[64] Experimentally, analysis of numerous mixtures of diverse model compounds, as well as mixtures of model compounds with asphaltenes, using the same methodology employed here demonstrates the detection of each component with comparable sensitivity.[25,28,57]

The L^2MS methodology employed here is similar to that employed previously. A small amount of asphaltenes is fixed on a sample platter and transferred into the vacuum chamber through a vacuum interlock. A pulse of IR light from a CO2 laser (λ = 10.6 μm; Alltec GmbH, model AL 882 APS) is focused to a spot (~50 μm in diameter) on the sample surface using a Cassegrainian microscope objective (Ealing Optics, 15×). Desorbed neutral molecules from the platter surface form a plume in the extraction region during a time of 10−50 μs. This plume is then intersected perpendicularly by the VUV output of a pulsed F2 excimer laser (λ = 157 nm; Coherent, Inc., ExciStar XS 200, Selmsdorf, Germany), and molecules are ionized through single-photon ionization (SPI). The resulting ions are mass-analyzed in a home-built time-of-flight mass spectrometer (TOF-MS) employing a modified Wiley−McLaren geometry. A dual microchannel plate

DOI: 10.1021/acs.energyfuels.7b01420
Energy Fuels 2017, 31, 9140−9151

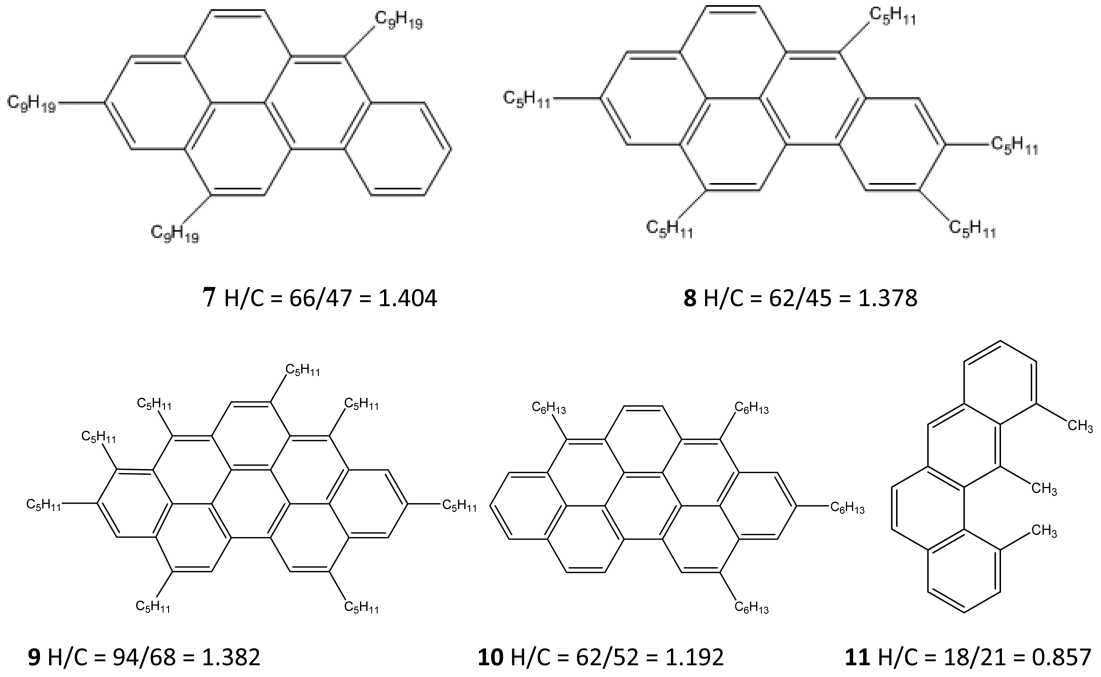

Figure 2. Second set of asphaltene model compounds (**7**–**9**, ISA; **10**, PA; **11**, CDA).

(MCP; 20 cm^2 active area; Burle Electro-Optics, Sturbridge, MA) set in a chevron configuration coupled with a large collector anode (Galileo TOF-4000) is used as a detector. Each recorded spectrum is averaged over 50 laser shots.

The SALDI-MS method of measuring asphaltene nanoaggregate weight has also been described previously.[27,44,59−61] When low laser pulse energies are employed, this method of measuring asphaltenes does not suppress aggregation, such that asphaltenes are detected as nanoaggregates.[28] This section provides a brief description of the apparatus. SALDI−MS mass spectra were obtained using a PCS4000 mass spectrometer with nonselective normal-phase NP20 arrays (Ciphergen, Fremont, CA). The surface of the array, composed of aluminum, was modified by the addition of silicon oxide groups. Mass spectra were acquired using a pulsed nitrogen laser with a wavelength of 337 nm. The laser pulse energy was scanned from 1000 to 6000 nJ in steps of 500 nJ for petroleum asphaltenes and from 1200 to 4800 nJ in steps of 400 nJ for coal asphaltenes. The mass spectra were externally calibrated using a standard mixture of low-molecular-weight peptides (Bio-Rad). Data were acquired in the positive-ion mode from m/z 0 to 20 000 Da, focused at 4000 Da. In SALDI−MS experiments, all asphaltenes were dissolved in toluene to form solutions with concentrations of 2 and 0.67 mg/mL. These solutions were used to obtain surface concentrations of 32 and 96 $\mu g/cm^2$ by depositing a drop of 2 μL solution onto a spot (outer diameter of 2.3 mm) on the sample substrate. The surface concentration of 288 $\mu g/cm^2$ was obtained by depositing 2 μL solution of 2 mg/mL three times after the previous drop was dried.

Computational Ensemble Analysis. Initial modeling was performed on molecules containing 5 and 8 fused aromatic rings and containing varying amounts of alkylation (Figure 1). These molecules were chosen to probe fused aromatic ring size (**1**−**3** vs **4**−**6**) and the effects of alkyl chain length.

We utilized CLUSTER v1.3 to sample the conformational space of ensembles containing 5 molecules each of **1**−**6**.[65] Initial clusters were obtained via a random arrangement of 5 molecules followed by genetic mutation to increase the diversity (and subsequent sampling) of the population of structures. These clusters were subsequently geometry optimized using molecular mechanics and semiempirical characterization. We utilized the UFF[66] and PM7[67,68] methodologies. The UFF (Universal Force Field) method is a computationally efficient molecular mechanics approach using parameters based upon the atom type, connectivity and hybridization. The PM7 method is a semiempirical approach based on the Hartree−Fock method that uses parameters obtained from experimental or high level *ab initio* data to approximate computationally intensive aspects of the calculations. Both the UFF and PM7 optimizations were performed in the gas phase to correspond with the experimental work described above.

Our second set of compounds (Figure 2) was designed using more compositionally accurate data obtained from the spectroscopy experiments (Tables 1 and 3). This second set of compounds included different length and quantity of alkyl chains tuned to match the compositional data from the ISA Eagle-Ford sample (**7**−**9**), the PA BG5 sample (**10**), and the CDA Adaro Coal sample (**11**). Cluster v1.3 was used to generate a diverse set of initial clusters containing 5 copies of each these molecules that were then subjected to geometry optimization in the gas phase using the UFF method.

Table 1. Experimental Compositional Data Showing Ratio of Elements for the ISA, PA, and CDA Asphaltene Samples[a]

sample	carbon	hydrogen	nitrogen	sulfur	oxygen	H/C ratio
ISA-Eagle Ford	73.24	8.5	1.69	9.69	6.53	1.39
PA-BG5	79.2	7.82	0.98	7.61	2.45	1.18
PA-UG8	81.07	7.11	1.02	8.94	1.6	1.05
CDA-Adaro	87.29	5.9	1.57	0.09	5.25	0.81
CDA-Wyoming	85.85	5.4	1.46	0.14	4.44	0.75

[a]C, H, N, and S abundances were measured by combustion, and O was measured by pyrolysis. These three types are very different especially in terms of H/C ratio.

We also simulated the dynamics of nanoaggregation using Molecular Dynamics with the AMBER molecular dynamics package.[69,70] The simulations were performed using either AMBER 14[69] or AMBER 16.[70] In all cases, partial charges were obtained via antechamber with HF/6-31G and parameters from the GAFF force field[71] were utilized while maintaining a constant temperature of 300 K. Solvent was not included in these simulations to probe directly the gas-phase interactions occurring in the experiments above. It should be noted that for the classical force fields (UFF, AMBER) used in this study the relative enthalpies should provide qualitatively accurate information. Where possible, we have confirmed classical enthalpies

DOI: 10.1021/acs.energyfuels.7b01420
Energy Fuels 2017, 31, 9140−9151

using quantum methods. Our initial MD structures were obtained by arranging 25 copies of **1**−**6** regularly in a grid. We then kept every fifth molecule generating starting structures where 5 molecules of **1**−**6** were well-separated (6−30 Å) in a box. These randomly spaced starting structures allowed us to model the process of aggregation. Each molecular simulation contained one type of asphaltene, i.e., we did not investigate mixtures. In addition to the MD simulations described above where we invested a significant amount of simulation time following aggregation from very well-spaced initial ensembles, we also investigated the process of aggregation starting from more closely spaced (7 Å) but still randomly aligned initial structures. We performed this test using molecules **9**−**11**.

For clusters of **1**−**6**, all steps of MD were performed using the CPU *sander* code of AMBER 14.[69] For clusters of **9**−**11**, all steps of MD were performed using the GPU-accelerated *pmemd* code of AMBER 16.[70,72,73] All the initial structures were minimized, then subjected to unrestrained MD. A single stage energy minimization process was performed without positional atomic restraints over a total of 500 steps. The first 250 steps were of steepest descent minimization before conjugate gradient minimization was executed on the remaining 250 steps. Once minimized, unrestrained MD at constant temperature (300 K) was performed with a 1 fs time-step and 999 Å nonbonded cutoff distance. Three different random seeds were used to initiate simulations of each cluster in order to speed surface coverage. A seed represents the set of initial velocities assigned to each atom at the beginning of the simulation. Simulations of clusters of **1**−**6** were run until aggregation or dissociation was observed, while simulations of clusters of **9**−**11** were run for a full 1.0 μs of *in vacuo* MD.

In the simulations containing **9**−**11**, all trajectories ended with all 5 molecules aggregated (Table 2). AMBER's *cpptraj* analysis tool was used to cluster the molecular dynamics trajectories into conformationally similar families using the hierarchical agglomerative clustering method.[74] This method was chosen since it is especially useful when the exact family count is unknown in advance. The clustering is based on an atomic coordinate RMSD distance metric. It is useful to use *cpptraj* for this analysis since both frame-by-frame cluster summaries and a representative conformation for each family are provided. Structural families with a greater than 5% representation in the overall ensemble were considered significant. AMBER energies were averaged over each trajectory and these average values were averaged together to obtain the overall average enthalpy reported below.

Center of mass distances were calculated using *cpptraj* included in AmberTools 16.[70] Entropy values were calculated using AMBER's *MMPBSA.py* utility by calculating the vibrational frequencies of the normal modes along various minima on the potential energy surface.[75] When entropy is approximated using the normal-mode analysis, and included in the overall free energy values, computational results are scaled to more experimentally realistic relative values.[76] Structures and trajectories were visualized using VMD.[77]

As an initial test of the accuracy of the AMBER results, we also selected the 5 lowest energy structures from each MD ensemble of **11** and compared the single-point and geometry optimized energies and structures with results from the semiempirical PM7 precise method in the MOPAC program,[68] and with the Global Hybrid Meta-GGA (M062X[78]) density functional with the 6-31G* basis set available in the Q-Chem v4.4 program.[79]

RESULTS AND DISCUSSION

Mass Spectrometry. Figure 3 shows the results from the determination of molecular weight by L^2MS and nanoaggregate weight by SALDI-MS for the diverse asphaltene samples. The molecular weight for the PAs and CDAs are similar to previous determinations by a variety of measurements. The molecular weight of the ISA (from the Eagle Ford formation) is similar to the molecular weight of another ISA from the Green River formation.[61] For a given sample, by dividing the nanoaggregate weight by the molecular weight, one obtains the aggregation number. Table 3 lists the (number-average) molecular weights and the (number-average) nanoaggregate weights as well as the aggregation numbers for the different samples. The molecular weight of the ISA shows a somewhat broader range and lighter centroid compared to the PAs. As expected, the CDAs show a much smaller molecular weight as well as a correspondingly narrower range of molecular weights. For each sample and class of samples, the nanoaggregate weights are well-defined and exhibit ranges that are comparable to the corresponding molecular weights.

The aggregation numbers of all samples are below 10, thus are very small. Moreover, the aggregation numbers of all asphaltene classes are very similar, roughly 7. Previous determinations of the critical nanoaggregate concentrations of PAs and CDAs showed that they are very similar.[38] Consistently, a series of asphaltenes spanning a range of thermal maturities was found to have a wide variety of chemical compositions (including different H/C ratios and molecular weights) but similar aggregate numbers.[61] Evidently, nanoaggregate properties for diverse asphaltenes are very similar, which aligns with the identity of the same solvency properties of these asphaltenes: asphaltenes have a balance of intermolecular forces that results in their being soluble in toluene but insoluble in heptane (according to their definition),

Table 2. Duration of the Molecular Dynamics Simulations of Compounds 1−6, 9−11, and the Number of Asphaltene Molecules That Aggregated[a]

compound	seed	simulation time (ns)	# in aggregates
1	1	0.51	3
	2	1.12	3
	3	0.82	4
2	1	3.45	4
	2	3.31	4
	3	28.4	3 and 2
3	1	10.4	3
	2	25	3 and 2
	3	10.4	3
4	1	0.66	4
	2	102	5
	3	21.3	5
5	1	7.1	5
	2	5.2	2 and 2 and 1
	3	5.2	3 and 2
6	1	8.5	4 and 1
	2	10	5
	3	10	5
9	1	1000	5
	2	1000	5
	3	1000	5
10	1	1000	5
	2	1000	5
	3	1000	5
11	1	1000	5
	2	1000	5
	3	1000	5

[a]For instance, a "3" indicates that 3 out of 5 molecules formed a single aggregate. The designation "2 and 2 and 1" indicates that 2 molecules each formed 2 aggregates while 1 molecule remained separated. Simulations on molecules **9**−**11** were initiated using a script that oriented molecules 7 Å apart. Other simulations used 30 Å spacings. Microsecond trajectories for **9**−**11** were simulated using the GPU-accelerated AMBER16 software. **7** and **8** were not run with MD because they are similar in structure to **2** and **5**.

DOI: 10.1021/acs.energyfuels.7b01420
Energy Fuels 2017, 31, 9140−9151

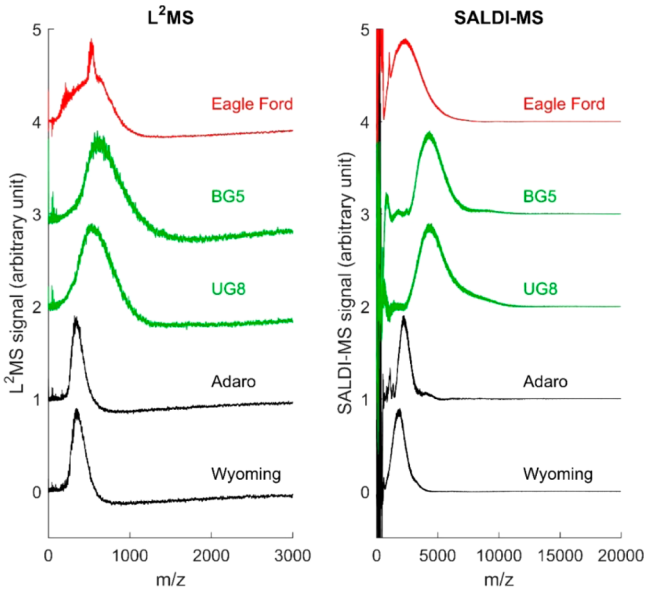

Figure 3. Left: Molecular weight of different asphaltenes by L^2MS. Right: Nanoaggregate weight of different asphaltenes by SALDI MS. The Eagle Ford sample is an ISA, the BG5 and UG8 samples are PAs, and the Adaro and Wyoming samples are CDAs.

Table 3. Experimental Aggregation Data for ISA, PA, and CDA Samples

sample	molecule weight (g/mol)	nanoaggregate weight (g/mol)	aggregate number
ISA-Eagle Ford	528	2969	5.6
PA-BG5	646	4983	7.7
PA-UG8	582	5361	9.2
CDA-Adaro	367	2455	6.7
CDA-Wyoming	377	1921	5.1

and that balance of intermolecular forces also controls their aggregation.

The similarity of the aggregation numbers does not mean all chemical properties are invariant. Indeed, the ISAs are dominated by aliphatic carbon while the CDAs are dominated by aromatic carbon and the PAs are intermediate. Nevertheless, steric hindrance should be a key factor on differing enthalpy and entropy of nanoaggregate formation. In particular, the different alkane fractions would impact steric hindrance and thus impact the structure of nanoaggregates. Previously, small temperature variation of CNAC for nanoaggregate formation have been reported.[20,42] As discussed in these papers, the implication is that nanoaggregate formation occurs in large measure as an entropic effect; the solvent entropy increases more than the asphaltene entropy decreases upon nanoaggregate formation. Independent of the driving force to form nanoaggregates, the molecules will generally orient in a nanoaggregate to optimize the enthalpy of interaction.

Similar entropy effects are well-known for micelle formation in aqueous systems.[80] For micelles in aqueous systems, the enthalpy of formation of ionic surfactants is positive due to incomplete neutralization of charge in the bilayer of the micelle, and the entropy change must override these countervailing enthalpic effects.[81] Consequently, the critical micelle concentrations (CMC) of ionic surfactants are larger than those of nonionic surfactants in aqueous systems.[81] The reduction of Gibbs free energy of micelle formation from Coulomb repulsion generally causes CMCs of ionic surfactants to be higher than for nonionic surfactants; asphaltenes are largely nonionic. While the systems are rather different, the CNAC of asphaltenes in toluene are comparable to CMCs of nonionic surfacants in aqueous systems.

Computational Modeling. We explored nanoaggregate structures of alkylaromatics as model compounds of asphaltenes using two computational approaches: a time-independent random sampling of conformational space with UFF enthalpy refinement as well as a time-dependent Molecular Dynamics approach to simulate initial aggregation and cluster dynamics. The dominance of the polarizability term of the Hansen parameters for asphaltenes supports these proposed models; there is no dominant H-bonding or polar effect in asphaltenes that would then necessitate heteroatom concerns.[82−84]

1. Random Search of Intermolecular Space and Energy Refinement with UFF. The Cluster program was used to sample intermolecular conformational space followed by the determination of low enthalpy conformations using the UFF force field.[66] Table 4 shows the number of unique minima and

Table 4. Conformational Enthalpies of 1−11 Obtained with the UFF Force Field in the Gas Phase

molecule	H/C ratio	# of min	enthalpy range (kcal/mol)	enthalpy min (kcal/mol)	enthalpy max (kcal/mol)	number of families
1	0.60	50	21.96	112.75	134.71	5
2	1.44	42	92.87	208.60	301.47	5
3	1.65	58	99.83	248.67	348.50	2
4	0.50	63	43.56	192.98	236.53	4
5	1.40	40	99.51	380.77	480.28	4
6	1.62	15	98.48	305.25	403.73	4
7	1.40	62	84.86	148.51	233.37	
8	1.38	42	100.22	241.50	341.72	4
9	1.38	42	96.56	491.74	588.30	3
10	1.19	90	98.42	252.95	351.38	4
11	0.86	78	34.96	151.42	186.38	5

enthalpy ranges for each asphaltene **1**−**11** using the UFF method. The enthalpy range corresponds to the difference in energy between the lowest energy aggregate and the highest energy aggregate in the ensemble. Table 4 provides information about the complexity of the gas-phase enthalpic surface for each model compound. The ensembles of low energy minima obtained on the UFF surface were also clustered into geometrically similar families using the hierarchical agglomerative clustering method available in the cpptraj module of AMBER 14.[69]

It should be noted that the enthalpies in Table 4 correspond to conformational enthalpies and not binding energies, i.e., these are the enthalpies associated with low energy geometric arrangements of 5 molecules each of **1**−**11**. The UFF enthalpy range is small for compounds **1** and **4** without alkyl arms and also for **11** with short alkyl arms. The number of unique minima for **1**−**11** on the UFF surface ranges from 15 to 90. Asphaltene **6** with an 8 fused ring core and dodecyl arms is surprisingly the least conformationally diverse ensemble with only 15 unique conformations. This may be indicative of the difficulty of arranging long flexible arms into a tight space. The number of conformational families for each ensemble is similar to most molecules containing 4 or 5 representative

DOI: 10.1021/acs.energyfuels.7b01420
Energy Fuels 2017, 31, 9140−9151

conformations. The two lowest enthalpy conformations for clusters of **1** are shown in Figure 4.

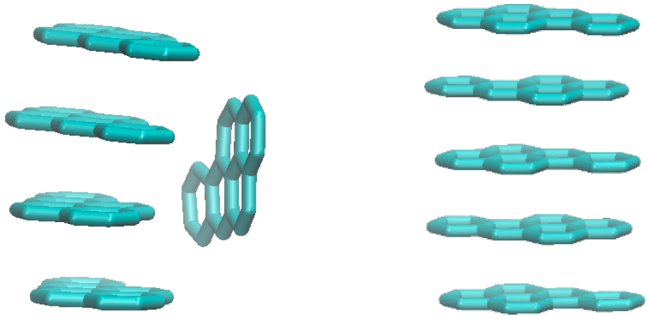

Figure 4. Lowest enthalpy conformation (left) and the second lowest enthalpy conformation of **1** (right) obtained with the UFF method.

In the lowest enthalpy structure (Figure 4), four molecules of **1** form face-to-face, pancake-like $\pi-\pi$ stacking interactions. This sandwich structure is stabilized by the favorable dispersion interactions involving the polarizable aromatic rings. The fifth molecule adopts a T-shaped geometry ($\pi-\sigma$ or quadrupolar interaction), which is stabilized by quadrupolar interactions and alkane polarizability. This structure is consistent with that observed in benzene dimers, i.e., the quadrupole driven T-shape dimer is slightly more stable than the slipped parallel or sandwich structure that arises due to the polarizability of the π electrons.[84] In the second lowest energy structure, five molecules of **1** form a perfectly $\pi-\pi$ sandwich cluster. However, there is only a 0.06 kcal/mol energetic difference between the two lowest conformations indicating that in the gas phase these structures are iso-energetic.

The lowest enthalpy structures from the UFF ensembles of **1**−**11** are shown in Figure 5 and Figure 6. Compounds without alkyl arms, or with short alkyl arms, such as **1**, **4**, and **11**, have low energy structures with dominant $\pi-\pi$ stacking interactions, suggesting the enthalpic component of aggregation is driven primarily by dispersion interactions among the π electrons. Compounds with relatively shorter alkyl arms, such as **2**, **8**, and **10**, adopt staggered π-stacking interactions, i.e., the planes of the fused aromatic rings are displaced or slipped some distance away from a perfectly stacked arrangement. We see that with an increase in the alkyl arm length, such as compounds **5** and **9**, the intermolecular geometries change to offset π-stacked interactions, or display partly staggered π-stacking interactions as in compound **5**. There are two types of interactions in the compounds (molecules **3**, **6**, **7**) with long alkyl arms: staggered π-stacked interactions and edge-on or T-shaped geometries. Most clusters typically form $\pi-\pi$ stacking interactions between 2 or 3 fragments, then form edge-on or T-shaped interaction with the remainder.

The ensemble of **3** contained 58 minima ranging over almost 100 kcal/mol but clustered into only 2 families. This indicates that the conformational diversity of **3** is smaller. This was a bit surprising considering that **3** contains dodecyl arms but also reflects the difficulty associated with packing long flexible arms into a tight space.

Figure 5 and especially Figure 6 clearly show the effect of increased alkane substitution on the increase disorder of π-stacking. With excessive alkane carbon such as for the ISA (**9**), the planar approach of two PAHs is largely precluded, reducing the stabilization due to dispersion interactions. As a result, the

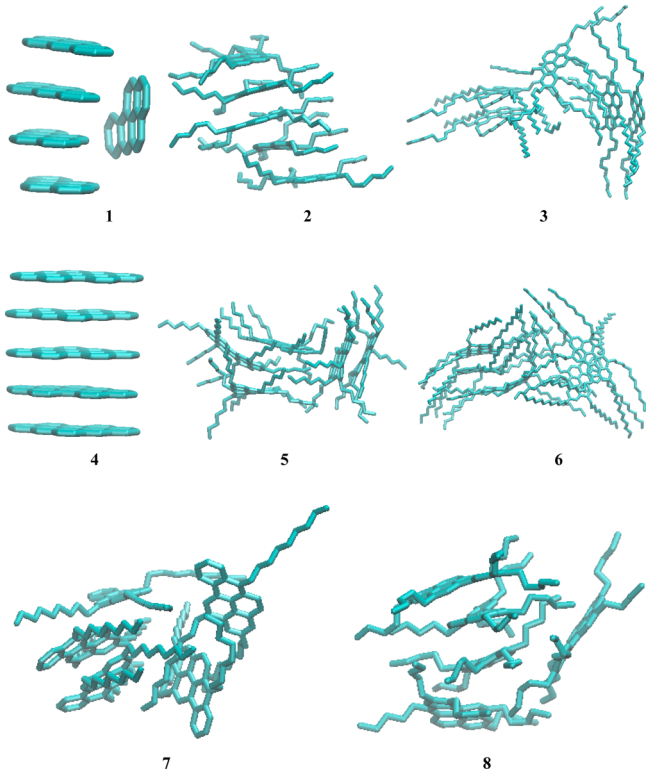

Figure 5. Low energy UFF "asphaltene" clusters for a variety of alkylaromatics.

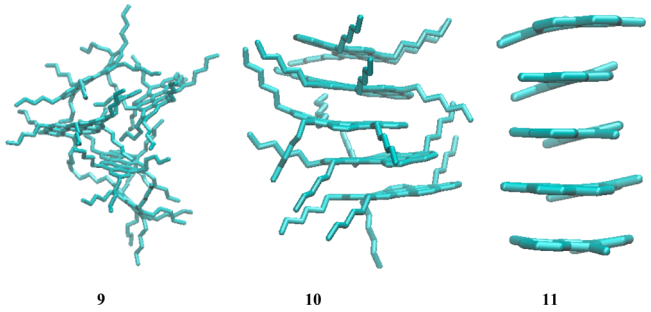

Figure 6. Low energy UFF asphaltene clusters for **9** ISA, **10** PA, and **11** CDA.

aggregate structure bears little resemblance to an ordered stack. For a moderate alkane fraction such as for PA (**10**), a disordered π-stack is seen. For very little alkane such as with CDAs (**11**), attractive dispersion interactions between aromatic ring systems can proceed unencumbered, resulting in a highly ordered stack. Related experimental results have recently been reported in agreement with these results. Ultrahigh resolution molecular imaging using AFM and STM are performed by transferring molecules of interest to a surface. Molecules that are planar provide excellent opportunity for imaging while molecules that are more three-dimensional are not imaged as well. In addition, the relatively rigid 2-D framework of PAHs enables excellent imaging while the alkanes can be more randomly oriented and not imaged as well. For CDAs that are largely planar with a high fraction of aromatic carbon, the AFM and STM images allowed identification of almost every carbon atom.[33] The PAs gave adequate imaging but the alkanes did compromise the images somewhat.[33,34] In order to validate island molecular architecture, STM was quite successfully used

DOI: 10.1021/acs.energyfuels.7b01420
Energy Fuels 2017, 31, 9140−9151

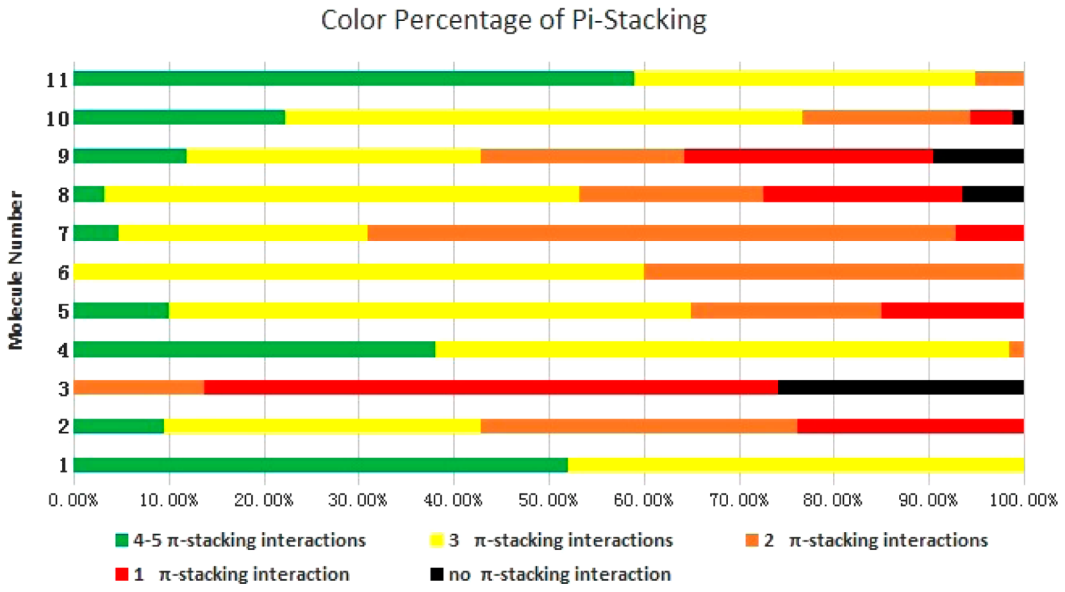

Figure 7. Percentage and types of π-stacking interactions found in the UFF ensembles of **1**−**11**. (Green: strongest π-stacking interactions including nearly perfectly 5 π-stacked or 4 π-stacked; yellow: 3 π-stacking interactions; orange: 2 π-stacking interactions; red: 1 π-stacking interaction; black: no π-stacking interactions. Clusters represented by red and black contain only σ−σ interactions.

to image the molecular orbitals and matched corresponding molecular orbital calculations. In addition, individual molecules were manipulated with the probe tip to determine the ability to rotate molecular segments around bonds (thus single bonds).[33,34] The ISA molecules were the most difficult to resolve due to the 3-D nature of the molecules and the related large fraction of alkane carbon.[34] These imaging results align closely with the structures in Figures 5 and 6.

We analyzed the type and degree of π-stacking in the UFF ensembles of **1**−**11** (Figures 5 and 6) in Figure 7. We see that molecules **1**, **4**, and **11**, that either lack alkyl arms or contain very short arms, modeling CDAs, form cluster ensembles in which the greatest percent of the conformations adopt perfectly π-stacked sandwich structures with 4 or 5 constituents. Molecule **3** with an 8 fused ring core and dodecyl arms, modeling ISAs, is least likely to form sandwich structures; when those structures occur, it is typically only between 2 constituents forming the least amount of π-stacking. Molecules with longer arms (**6**, **7**, and **8**) adopt conformations with the largest percentage of T-shaped clusters aggregated to sandwiches containing 3 constituents.

2. Simulating Asphaltene Aggregation Using Molecular Dynamics. The AMBER Molecular Dynamics package was used to simulate the process of aggregation for most structures **1**−**11**. Simulation times varied as shown in Table 2. We clustered the resulting AMBER ensembles into geometrically similar families to assess the diversity of the clusters formed. We approximated the overall enthalpy using gas-phase AMBER energies. We estimated the entropy by calculating the vibrational frequencies of normal modes at minima along the potential energy surface using MMPBSA.py.[75,85]

This is a difficult task; moreover, the results here are for vacuum, and solvent effects are important for nanoaggregate formation. It is also important to note that when using classical force fields such as UFF and AMBER, the relative energies/enthalpies have been shown to provide physically meaningful results; however, the absolute energies do not.[86] Coarse grain modeling of asphaltene molecules at the oil-water interfaces indicated related agreement; the PAH of the asphaltenes is in plane while the alkanes remain in the organic phase,[87] which is all confirmed in experiment.[32] Preliminary structural and energetic comparisons between the AMBER minima and a variety of quantum mechanically optimized results suggest that the classical structures are in agreement with quantum results, and the energetic ordering of minimum energy structures is correct; however, the relative AMBER energies need correction. The quantum calculations are computationally very intense—work is underway to generate a large enough data set for scaling the classical enthalpies. Thus, we view these results as being qualitative. We see narrow ranges of conformational diversity in the AMBER ensembles, relative to the UFF ensembles. This is particularly so for **1**−**6** and may be related to the short simulation times for these clusters. For **9**−**11** we were able to run MD for 1 μs and in those systems we see very similar conformational flexibility with all ensembles clustering into 3−5 families regardless of structure.

It is not surprising that the classical force field based enthalpies are all positive values suggesting a lack of spontaneous formation in the gas phase. This is due to the computationally efficient yet simplistic formalism underlying molecular mechanics, and in this case, in particular, the lack of inclusion of solvent effects. We can draw some qualitative understanding from these results. For instance, comparing the overall resulting free energies for **9**−**11**; we see that **9** (with 8 fused rings and 8 pentyl arms) has the least favorable enthalpy but the largest entropy while **11** (with 4 fused rings and 4 hexyl arms) has the smallest enthalpy and entropy values. This would suggest that the alkyl arms are contributing significantly to the overall energetics (comparing **9** to **10**) but the number of rings has a smaller effect (comparing **10** to **11**). This analysis is further supported by the low energy structures shown in Figure 6. Compound **11** is very neatly packed with clear π-stacking driving the overall structure of the cluster. As the arms increase in length, the aggregated complex (although still aggregated), shows less clear, organized noncovalent interactions between asphaltenes. It is this lack of defined, consistent interactions

DOI: 10.1021/acs.energyfuels.7b01420
Energy Fuels 2017, 31, 9140−9151

between molecules that likely contributes to the higher ΔG values for the compounds with larger alkyl arms. The increased length of the alkyl chains shows a clear increase in the entropy (as expected), but likely does not help in structurally stabilizing the aggregated complex. The MD simulations from well-separated initial structures (Table 2) suggest that the length of the arms did not substantially change the time it took for aggregation to occur, but the presence of alkyl arms may affect the overall energetic stability of the aggregates once formed.

Table 5 shows that the enthalpy terms are very roughly twice the magnitude of the entropy terms with the (vacuum) enthalpy being large. In addition, with more alkane substitution, the entropy effects become larger. How this translates to solution chemistry is a subject of current investigation.

Given the longer simulation times available for **9**–**11**, we further analyzed the ensembles by measuring the center of mass distances between the molecules throughout the simulation. The initial clusters contained well-separated constituents and after ∼200 ns of simulation had aggregated into an almost perfectly π-stacked motif, in spite of the hexyl arms that emanate from the 8 membered fused ring core. The data shown in Figure 8 is representative of all the data that was obtained for structures **9** (ISA), **10** (PA), and **11**, CDA.

Table 5. Number of Conformational Families, AMBER Enthalpies and Entropies Averaged over the 3 Trajectories, and Resulting Free Energies of Ensembles of 1–11[a]

molecule	number of families					
trajectory	1	2	3	ΔH – average AMBER enthalpies	average $T\Delta S$	ΔG
1	10	8	5	220.8		
2	5	6	3	467.1		
3	7	7	1	881.3		
4	9	4	6	433.7		
5	3	9	7	956.4		
6	7	5	2	1867.8		
9 (ISA)	5	4	4	1026.9	484.8	542.1
10 (PA)	3	3	5	646.0	346.0	300.0
11 (CDA)	3	4	5	356.5	130.0	226.5

[a]All energies are in kcal/mol. (**7** and **8** were not run because they are similar to **2** and **5**.)

CONCLUSIONS

Asphaltenes from diverse origins are examined herein: coal-derived asphaltenes (CDAs), petroleum asphaltenes (PAs), and immature source-rock asphaltenes (ISAs). By definition, all these samples have the same solubility characteristics; nevertheless, these classes of asphaltenes span a large range of elemental composition with the H:C ratio varying from roughly 0.8 for CDAs (dominated by aromatic carbon), 1.1 for PAs (comparable abundances of aromatic and aliphatic carbon), to 1.4 for ISAs (dominated by aliphatic carbon). Mass spectrometry measurements show that all these diverse asphaltenes form nanoaggregates and that all aggregation numbers are similar and about 7. In that nanoaggregate formation relates to intermolecular interaction and thus relates to solution behavior, the identical solubility characteristics of asphaltenes correlate to similarity in nanoaggregate properties. Nevertheless, the large difference in alkane fraction for these different asphaltenes mandates differences in steric repulsion and consequently the extent of order in the nanoaggregate.

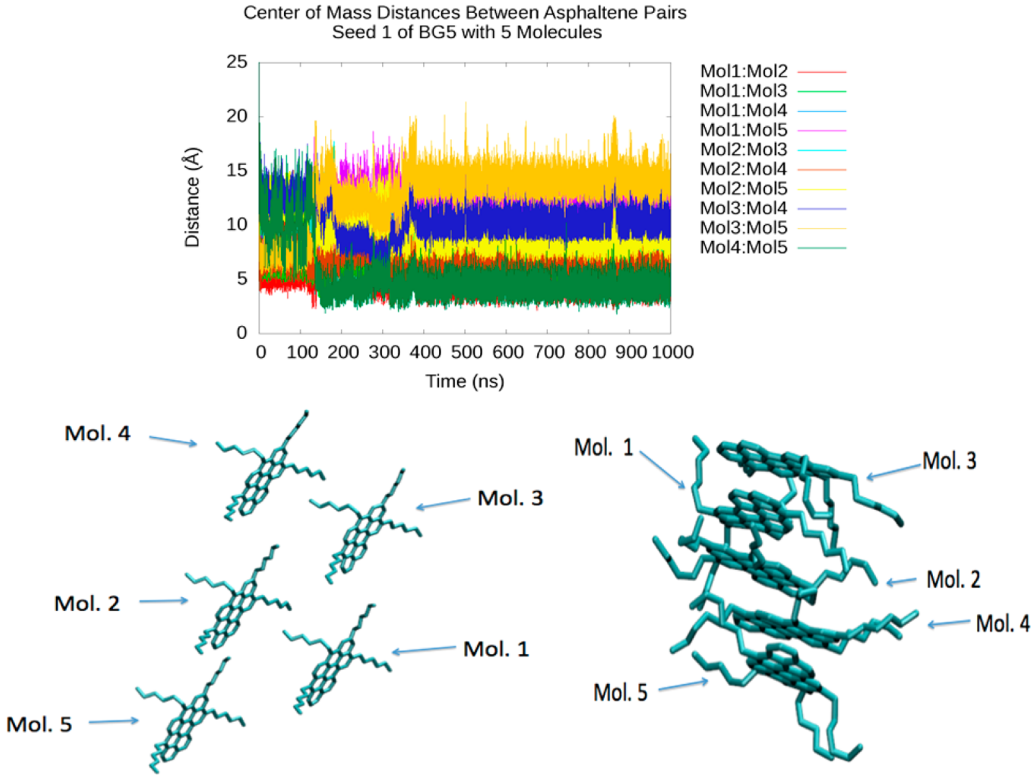

Figure 8. Center of mass distances between 5 BG5 asphaltenes (top); Initial spacing of the BG5 structures (left); BG5 aggregated with each other in the last frame of the simulation (right). BG5 corresponds to compound **10** in Figure 4.

DOI: 10.1021/acs.energyfuels.7b01420
Energy Fuels 2017, 31, 9140–9151

Molecular dynamics simulations on selected molecular structures was used to probe nanoaggregates. For CDAs with a small alkane fraction, nanoaggregate π-stacking is very ordered; for PAs with their moderate alkane fraction, nanoaggregate π-stacking is disordered as gleaned in Figure 7. For ISAs with their large alkane fraction, π-stacking is almost precluded. These results are consistent with recent ultrahigh resolution imaging of the same asphaltenes.[33,34]

AUTHOR INFORMATION

Corresponding Author

*E-mail: mullins1@slb.com.

ORCID

Cooper Taylor: 0000-0003-0617-2009

Oliver C. Mullins: 0000-0001-6951-9415

Present Address

[¶]Key Laboratory of Separation Science for Analytical Chemistry, Dalian Institute of Chemical Physics, Chinese Academy of Sciences, Dalian 116023, People's Republic of China

Notes

The authors declare no competing financial interest.

ACKNOWLEDGMENTS

The authors would like to thank the Visiting Scholar Program of the Chinese Academy of Science for supporting this project. We would like to thank Taras Bryndzia of Shell International Exploration and Production Inc. for providing the material used to extract the ISAs. We would like to thank John C. Whitin of Stanford University and Haiyang Li of the Dalian Institute of Chemical Physics for assistance with the experiments.

REFERENCES

(1) Mullins, O. C.; Sheu, E. Y.; Hammami, A.; Marshall, A. G., Eds. *Asphaltenes, Heavy Oil and Petroleomics*; Springer: New York, 2007.

(2) Mullins, O. C. The Modified Yen Model. *Energy Fuels* **2010**, *24*, 2179−2207.

(3) Mullins, O. C.; Sabbah, H.; Eyssautier, J.; Pomerantz, A. E.; Barré, L.; Andrews, A. B.; Ruiz-Morales, Y.; Mostowfi, F.; McFarlane, R.; Goual, L.; Lepkowicz, R.; Cooper, T.; Orbulescu, J.; Leblanc, J. M.; Edwards, J.; Zare, R. N. Advances in Asphaltene Science and the Yen-Mullins Model. *Energy Fuels* **2012**, *26*, 3986−4003.

(4) Hammami, A.; Ratulowski, J. Precipitation and Deposition of Asphaltenes in Production Systems: A Flow Assurance Overview. In *Asphaltenes, Heavy Oil and Petroleomics*; Springer: New York, 2007; Chapter 13.

(5) Mullins, O. C.; Di Primio, R.; Steve Uchytil, S.; Zuo, J. Y.; Dumont, H.; Mishra, V.; Pfeiffer, T.; Achourov, V. Bitumen And Tar Deposition And Tar Mat Formation Accounted For By Multiple Charging, Trap Filling and Reservoir Fluid Geodynamics; SPE 181544; ATCE, Dubai, 2016.

(6) Pfeiffer, T.; Di Primio, R.; Vladislav Achourov, V.; Mullins, O. C. Scanning Electron Micrographs of Tar Mat Intervals Formed by Asphaltene Phase Transition. *Petrophysics* **2017**, *58*, 141−152.

(7) Zuo, J.; Pan, S.; Wang, K.; Mullins, O. C.; Dumont, H.; Chen, L.; Mishra, V.; Canas, J. Analysis of Asphaltene Instability Using Diffusive and Thermodynamic Models during Gas Charges into Oil Reservoirs. *Energy Fuels* **2017**, *31*, 3717.

(8) Freed, D. E.; Mullins, O. C.; Zuo, J. Y. Asphaltene gradients in the presence of GOR gradients. *Energy Fuels* **2010**, *24* (7), 3942−3949.

(9) Zuo, J. Y.; Mullins, O. C.; Freed, D. E.; Dong, C.; Elshahawi, H.; Seifert, D. J. Advances in the Flory-Huggins-Zuo Equation of State for Asphaltene Gradients and Formation Evaluation. *Energy Fuels* **2013**, *27*, 1722−1735.

(10) Mullins, O. C.; Betancourt, S. S.; Cribbs, M. E.; Creek, J. L.; Andrews, A. B.; Dubost, F.; Venkataramanan, L. The colloidal structure of crude oil and the structure of reservoirs. *Energy Fuels* **2007**, *21*, 2785−2794.

(11) Mullins, O. C. *The Physics of Reservoir Fluids; Discovery through Downhole Fluid Analysis*; Schlumberger Press: Houston, TX, 2008.

(12) Mullins, O. C.; Di Primio, R.; Zuo, J. Y.; Uchytil, S.; Mishra, V. K.; Dumont, H.; Pfeiffer, T.; Achourov, V.; Pomerantz, A. E.; Forsythe, J.; Betancourt, S. S.; Dong, C.; Elshahawi, H. Reservoir Fluid Geodynamics; the Link between Petroleum Systems and Production Concerns Relating to Fluids and Tar Distributions in Reservoirs; SPE 181535; ATCE, Dubai, 2016.

(13) Zuo, J. Y.; Mullins, O. C.; Achourov, V.; Pfeiffer, T.; Pan, S.; Wang, K.; Kollien, T.; Di Primio, R. Fluid distributions during light hydrocarbon charges into oil reservoirs using multicomponent Maxwell-Stefan diffusivity in gravitational field. *Fuel* **2017**, *209*, 211−223.

(14) Groenzin, H.; Mullins, O. C. Asphaltene Molecular Size and Structure. *J. Phys. Chem. A* **1999**, *103*, 11237−11245.

(15) Groenzin, H.; Mullins, O. C. Molecular sizes of asphaltenes from different origin. *Energy Fuels* **2000**, *14*, 677.

(16) Buenrostro-Gonzalez, E.; Groenzin, H.; Lira-Galeana, C.; Mullins, O. C. The Overriding chemical principles that define asphaltenes. *Energy Fuels* **2001**, *15*, 972.

(17) Andrews, A. B.; Mullins, O. C.; Sen, P. N.; Guerra, R. E. Diffusivity of Asphaltene Molecules by Fluorescence Correlation Spectroscopy. *J. Phys. Chem. A* **2006**, *110*, 8093.

(18) Guerra, R.; Andrews, A. B.; Mullins, O. C.; Sen, P. N. Diffusivity of coal and petroleum asphaltene monomers by fluorescence correlation spectroscopy. *Fuel* **2007**, *86*, 2016−2020.

(19) Wargadalam, V. J.; Norinaga, K.; Iino, M. Size and shape of a coal asphaltene studied by viscosity and diffusion coefficient measurements. *Fuel* **2002**, *81*, 1403−1407.

(20) Freed, D. E.; Lisitza, N. V.; Sen, P. N.; Song, Y. Q. A study of asphaltene nanoaggregation by NMR. *Energy Fuels* **2009**, *23*, 1189−1193.

(21) Hortal, A. R.; Hurtado, P. M.; Martınez-Haya, B.; Mullins, O. C. Molecular weight distributions of coal and petroleum asphaltenes from laser desorption ionization experiments. *Energy Fuels* **2007**, *21*, 2863−2868.

(22) Pinkston, D. S.; Duan, P.; Gallardo, V. A.; Habicht, S. C.; Tan, X.; Qian, K.; Gray, M.; Muellen, K.; Kenttamaa, H. Analysis of asphaltenes and asphaltene model compounds by laser-induced acoustic desorption/Fourier transform ion cyclotron resonance mass spectrometry. *Energy Fuels* **2009**, *23*, 5564−5570.

(23) Pomerantz, A. E.; Hammond, M. R.; Morrow, A. L.; Mullins, O. C.; Zare, R. N. Two step laser mass spectrometry of asphaltenes. *J. Am. Chem. Soc.* **2008**, *130* (23), 7216−7217.

(24) Pomerantz, A. E.; Hammond, M. R.; Morrow, A. L.; Mullins, O. C.; Zare, R. N. Asphaltene Molecular Weight Distribution Determined by Two-Step Laser Mass Spectrometry. *Energy Fuels* **2009**, *23* (3), 1162−1168.

(25) Sabbah, H.; Morrow, A. L.; Pomerantz, A. E.; Zare, R. N. Evidence for island structures as the dominant architecture of asphaltenes. *Energy Fuels* **2011**, *25*, 1597−1604.

(26) Rodgers, R. P.; Marshall, A. G. Petroleomics: advanced characterization of petroleum derived materials by Fourier transform ion cyclotron resonance mass spectrometry (FT-ICR MS), In *Asphaltenes, Heavy Oil and Petroleomics*; Springer: New York, 2007; Chapter 3.

(27) Wu, Q.; Pomerantz, A. E.; Mullins, O. C.; Zare, R. N. Fragmentation and Aggregation in Laser Desorption Laser Ionization and Surface Assisted Laser Desorption Ionization Mass Spectrometry. *J. Am. Soc. Mass Spectrom.* **2013**, *24*, 1116−1122.

(28) Pomerantz, A. E.; Wu, Q.; Mullins, O. C.; Zare, R. N. Laser Based Mass Spectrometric Assessment of Asphaltene Molecular Weight, Molecular Architecture, and Nanoaggregate Number. *Energy Fuels* **2015**, *29*, 2833−2842.

DOI: 10.1021/acs.energyfuels.7b01420
Energy Fuels 2017, 31, 9140−9151

(29) Borton, D.; Pinkston, D. S.; Hurt, M. R.; Tan, X.; Azyat, K.; Tykwinski, R.; Gray, M.; Qian, K.; Kenttamaa, H. I. Molecular structures of asphaltenes based on the dissociation reactions of their ions in mass spectrometry. *Energy Fuels* **2010**, *24* (10), 5548−5559.
(30) Tang, W.; Hurt, M. R.; Sheng, H.; Riedeman, J. S.; Borton, D. J.; Slater, P.; Kenttämaa, H. I. Structural Comparison of Asphaltenes of Different Origins Using Multi-stage Tandem Mass Spectrometry. *Energy Fuels* **2015**, *29* (3), 1309−1314.
(31) Rane, J. P.; Zarkar, S.; Pauchard, V.; Mullins, O. C.; Christie, D.; Andrews, A. B.; Pomerantz, A. E.; Banerjee. Applicability of the Langmuir Equation of State for Asphaltene Adsorption at the Oil−Water Interface: Coal-Derived, Petroleum, and Synthetic Asphaltenes. *Energy Fuels* **2015**, *29* (6), 3584−3590.
(32) Andrews, A. B.; McClelland, A.; Korkeila, O.; Krummel, A.; Mullins, O. C.; Demidov, A.; Chen, Z. Sum frequency generation studies of Langmuir films of complex surfactants and asphaltenes. *Langmuir* **2011**, *27* (10), 6049−6058.
(33) Schuler, B.; Meyer, G.; Pena, D.; Mullins, O. C.; Gross, L. Unraveling the molecular structures of asphaltenes by atomic force microscopy. *J. Am. Chem. Soc.* **2015**, *137* (31), 9870−9876.
(34) Schuler, B.; Fatayer, S.; Meyer, G.; Rogel, E.; Moir, M.; Zhang, Y.; Harper, M. R.; Pomerantz, A. E.; Bake, K. D.; Witt, M.; Pena, D.; Kushnerick, J. D.; Mullins, O. C.; Ovalles, C.; van den Berg, F. G. A.; Gross, L. Heavy oil based mixtures of different origins and treatments studied by AFM. *Energy Fuels* **2017**, *31* (7), 6856−6861.
(35) Schuler, B.; Zhang, Y.; Collazos, S.; Fatayer, S.; Meyer, G.; Perez, D.; Guitian, E.; Harper, M. R.; Kushnerick, J. D.; Pena, D.; Gross, L. Characterizing aliphatic moieties in hydrocarbons with atomic force microscopy. *Chem. Sci.* **2017**, *8*, 2315−2320.
(36) Gray, M. Consistency of Asphaltene Chemical Structures with Pyrolysis and Coking Behavior. *Energy Fuels* **2003**, *17* (6), 1566−1569.
(37) Alshareef, A. H.; Scherer, A.; Tan, X.; Azyat, K.; Stryker, J. M.; Tykwinski, R. R.; Gray, M. R. Formation of archipelago structures during thermal cracking implicates a chemical mechanism for the formation of petroleum asphaltenes. *Energy Fuels* **2011**, *25*, 2130−2136.
(38) Andreatta, G.; Bostrom, N.; Mullins, O. C. High-Q Ultrasonic Determination of the Critical Nanoaggregate Concentration of Asphaltenes and the Critical Micelle Concentration of Standard Surfactants. *Langmuir* **2005**, *21*, 2728.
(39) Andreatta, G.; Goncalves, C. C.; Buffin, G.; Bostrom, N.; Quintella, C. M.; Arteaga-Larios, F.; Perez, E.; Mullins, O. C. Nanoaggregates and Structure-Function Relations in Asphaltenes. *Energy Fuels* **2005**, *19*, 1282−1289.
(40) Mostowfi, F.; Indo, K.; Mullins, O. C.; McFarlane, R. Asphaltene Nanoaggregates and the Critical Nanoaggregate Concentration from Centrifugation. *Energy Fuels* **2009**, *23*, 1194−1200.
(41) Zeng, H.; Song, Y. Q.; Johnson, D. L.; Mullins, O. C. Critical nanoaggregate concentration of asphaltenes by low frequency conductivity. *Energy Fuels* **2009**, *23*, 1201−1208.
(42) Goual, L.; Sedghi, M.; Zeng, H.; Mostowfi, F.; McFarlane, R.; Mullins, O. C. On the Formation and Properties of Asphaltene Nanoaggregates and Cluster by DC-Conductivity and Centrifugation. *Fuel* **2011**, *90*, 2480−2490.
(43) Indo, K.; Ratulowski, J.; Dindoruk, B.; Gao, J.; Zuo, J. Y.; Mullins, O. C. Asphaltene Nanoaggregates Measured in a Live Crude Oil by Centrifugation. *Energy Fuels* **2009**, *23*, 4460−4469.
(44) Wu, Q.; Pomerantz, A. E.; Mullins, O. C.; Zare, R. N. Laser-based Mass Spectrometric Determination of Aggregation Numbers for Petroleum- and Coal-Derived Asphaltenes. *Energy Fuels* **2014**, *28*, 475−482.
(45) Eyssautier, J.; Levitz, P.; Espinat, D.; Jestin, J.; Gummel, J.; Grillo, I.; Barre, L. Insight into asphaltene nanoaggregate structure inferred by small angle neutron and X-ray scattering. *J. Phys. Chem. B* **2011**, *115*, 6827−6837.
(46) Wang, H.; Xu, H.; Jia, W.; Liu, J.; Ren, S. Revealing the Intermolecular Interactions of Asphaltene Dimers by Quantum Chemical Calculations. *Energy Fuels* **2017**, *31*, 2488−2495.
(47) Sedghi, M.; Goual, L.; Welch, W.; Kubelka, J. Effect of Asphaltene Structure on Association and Aggregation Using Molecular Dynamics. *J. Phys. Chem. B* **2013**, *117*, 5765−5776.
(48) Sharma, A.; Groenzin, H.; Tomita, A.; Mullins, O. C. Probing Order in Asphaltenes and Aromatic Ring Systems by HRTEM. *Energy Fuels* **2002**, *16*, 490.
(49) Feng, Y.; Le Doan, T. V.; Pomerantz, A. E. The Chemical Composition of Bitumen in Pyrolyzed Green River Oil Shale: Characterization by ^{13}C NMR Spectroscopy. *Energy Fuels* **2013**, *27*, 7314−7323.
(50) Andrews, A. B.; Edwards, J. C.; Mullins, O. C.; Pomerantz, A. E. Comparison of Coal and Petroleum Asphaltenes by ^{13}C Nuclear Magnetic Resonance and DEPT. *Energy Fuels* **2011**, *25*, 3068−3076.
(51) Hirano, K. Outline of NEDOL coal liquefaction process development (pilot plant program). *Fuel Process. Technol.* **2000**, *62* (23), 109−118.
(52) Tissot, B. P.; Welte, D. H. *Petroleum Formation and Occurrence*; Springer-Verlag: Berlin, Germany, 1978.
(53) Rogel, E.; Ovalles, C.; Pomerantz, A. E.; Zuo, J. Y.; Mullins, O. C. The Impact of Solubility Parameter Measurements on Predicted Asphaltene Gradients. *Energy Fuels* **2016**, *30* (11), 9132−9140.
(54) Ikeda, K.; Sakawaki, K.; Nogami, Y.; et al. Kinetic evaluation of progress in coal liquefaction in the 1 t/d PSU for the NEDOL process. *Fuel* **2000**, *79* (3−4), 373−378.
(55) Pomerantz, A. E.; Bake, K. D.; Craddock, P. R.; Kurzenhauser, K. W.; Kodalen, B. G.; Mitra-Kirtley, S.; Bolin, T. Sulfur Speciation in Kerogen and Bitumen from Gas and Oil Shales. *Org. Geochem.* **2014**, *68*, 5−12.
(56) Sabbah, H.; Morrow, A. L.; Pomerantz, A. E.; Mullins, O. C.; Tan, X.; Gray, M. R.; Azyat, K.; Tykwinski, R. R.; Zare, R. N. Comparing Laser Desorption/Laser Ionization Mass Spectra of Asphaltenes and Model Compounds. *Energy Fuels* **2010**, *24*, 3589−3594.
(57) Sabbah, H.; Pomerantz, A. E.; Wagner, M.; Müllen, K.; Zare, R. N. Laser Desorption Single-Photon Ionization of Asphaltenes: Mass Range, Compound Sensitivity, and Matrix Effects. *Energy Fuels* **2012**, *26*, 3521−3526.
(58) Hurtado, P.; Gamez, F.; Martínez-Haya, B. One- and Two-Step Ultraviolet and Infrared Laser Desorption Ionization Mass Spectrometry of Asphaltenes. *Energy Fuels* **2010**, *24*, 6067−6073.
(59) Wu, Q.; Seifert, D. J.; Pomerantz, A. E.; Mullins, O. C.; Zare, R. N. Constant Asphaltene Molecular and Nanoaggregate Mass in a Gravitationally Segregated Reservoir. *Energy Fuels* **2014**, *28*, 3010−3015.
(60) Pomerantz, A. E. Toward Molecule-Specific Geochemistry of Heavy Ends: Application to the Upstream Oil Industry. *Ind. Eng. Chem. Res.* **2016**, *55*, 4403−4414.
(61) Pomerantz, A. E.; Le Doan, T. V.; Craddock, P. R.; Bake, K. D.; Kleinberg, R. L.; Burnham, A. K.; Wu, Q.; Zare, R. N.; Brodnik, G.; Lo, W. C. H.; Grayson, M.; Mitra-Kirtley, S.; Bolin, T. B.; Wu, T. Impact of Laboratory-Induced Thermal Maturity on Asphaltene Molecular Structure. *Energy Fuels* **2016**, *30*, 7025−7036.
(62) Hanley, L.; Zimmermann, R. Light and molecular ions: The emergence of vacuum UV single-photon ionization in MS. *Anal. Chem.* **2009**, *81*, 4174−4182.
(63) Maechling, C. R.; Clemett, S. J.; Engelke, F.; Zare, R. N. Evidence for thermalization of surface-desorbed molecules at heating rates of 10^8 K/s. *J. Chem. Phys.* **1996**, *104*, 8768−8776.
(64) de Hoffmann, E.; Stroobant, V. *Mass Spectrometry: Principles and Applications*, 3rd ed.; John Wiley & Sons, Ltd.: Chichester, U.K., 2007; p 489.
(65) Kanters, R. P.F.; Donald, K. J. CLUSTER: Searching for Unique Low Energy Minima of Structures Using a Novel Implementation of a Genetic Algorithm. *J. Chem. Theory Comput.* **2014**, *10*, 5729−5737.
(66) Rappé, A. K.; Casewit, C. J.; Colwell, K. S.; Goddard, W. A., III; Skiff, W. M. UFF, a full periodic-table force-field for molecular mechanics and molecular-dynamics simulations. *J. Am. Chem. Soc.* **1992**, *114* (25), 10024−10035.

DOI: 10.1021/acs.energyfuels.7b01420
Energy Fuels 2017, 31, 9140−9151

(67) Throssel, K.; Frisch, M. J. Evaluation and Improvement of Semi-empirical methods I: PM7R8: A variant of PM7 with numerically stable hydrogen bonding corrections, manuscript in preparation.
(68) Stewart, J. J. P. Optimization of parameters for semiempirical methods VI: more modifications to the NDDO approximations and re-optimization of parameters, J. Molec. *J. Mol. Model.* **2013**, *19*, 1−32.
(69) Case, D. A.; Babin, V.; Berryman, J. T.; Betz, R. M.; Cai, Q.; Cerutti, D. S.; Cheatham, I. T. E.; Darden, T. A.; Duke, R. E.; Gohlke, H.; Goetz, A. W.; Gusarov, S.; Homeyer, N.; Janowski, P.; Kaus, J.; Kolossváry, I.; Kovalenko, A.; Lee, T. S.; LeGrand, S.; Luchko, T.; Luo, R.; Madej, B.; Merz, K. M.; Paesani, F.; Roe, D. R.; Roitberg, A.; Sagui, C.; Salomon-Ferrer, R.; Seabra, G.; Simmerling, C. L.; Smith, W.; Swails, J.; Walker, R. C.; Wang, J.; Wolf, R. M.; Wu, X.; Kollman, P. A. *AMBER* v 14; University of California, San Francisco, 2014.
(70) Case, D. A.; Betz, R.M.; Cerutti, D.S.; Cheatham, T.E., III; Darden, T.A.; Duke, R.E.; Giese, T.J.; Gohlke, H.; Goetz, A.W.; Homeyer, N.; Izadi, S.; Janowski, P.; Kaus, J.; Kovalenko, A.; Lee, T.S.; LeGrand, S.; Li, P.; Lin, C.; Luchko, T.; Luo, R.; Madej, B.; Mermelstein, D.; Merz, K.M.; Monard, G.; Nguyen, H.; Nguyen, H.T.; Omelyan, I.; Onufriev, A.; Roe, D.R.; Roitberg, A.; Sagui, C.; Simmerling, C.L.; W. M., Botello-Smith, Swails, J.; Walker, R.C.; Wang, J.; Wolf, R.M.; Wu, X.; Xiao, L.; Kollman, P.A., *AMBER 2016*; University of California, San Francisco, 2016.
(71) Wang, J.; Wolf, R.; Caldwell, J.; Kollman, P.; Case, D. Development and testing of a general Amber force field. *J. Comput. Chem.* **2004**, *25*, 1157−1174.
(72) Goetz, A. W.; Williamson, M. J.; Xu, D.; Poole, D.; Le Grand, S.; Walker, R. C. Routine microsecond molecular dynamics simulations with AMBER - Part I: Generalized Born. *J. Chem. Theory Comput.* **2012**, *8* (5), 1542−1555.
(73) Le Grand, S.; Goetz, A. W.; Walker, R. C. SPFP: Speed without compromise - a mixed precision model for GPU accelerated molecular dynamics simulations. *Comput. Phys. Commun.* **2013**, *184*, 374−380.
(74) Roe, D. R.; Cheatham, T., III. PTRAJ and CPPTRAJ: Software for Processing and Analysis of Molecular Dynamics Trajectory Data. *J. Chem. Theory Comput.* **2013**, *9*, 3084−3095.
(75) Miller, B. R.; McGee, T. D.; Swails, J. M.; Homeyer, N.; Gohlke, H.; Roitberg, A. E. MMPBSA.py: An Efficient Program for End-State Free Energy Calculations. *J. Chem. Theory Comput.* **2012**, *8*, 3314−3321.
(76) Hou, T.; Wang, J.; Li, Y.; Wang, W. *J. Chem. Inf. Model.* **2010**, *50*, 55.
(77) Humphrey, W.; Dalke, A.; Schulten, K. *J. Mol. Graphics* **1996**, *14*, 33.
(78) Zhao, Y.; Truhlar, D. G. The M06 suite of density functionals for main group thermochemistry, thermochemical kinetics, noncovalent interactions, excited states, and transition elements: two new functionals and systematic testing of four M06-class functionals and 12 other functionals. *Theor. Chem. Acc.* **2008**, *120*, 215−241.
(79) Shao, Y.; Gan, Z.; Epifanovsky, E.; Gilbert, A. T. B.; Wormit, M.; Kussmann, J.; Lange, A. W.; Behn, A.; Deng, J.; Feng, X.; Ghosh, D.; Goldey, M.; Horn, P. R.; Jacobson, L. D.; Kaliman, I.; Khaliullin, R. Z.; Kuś, T.; Landau, A.; Liu, J.; Proynov, E. I.; Rhee, Y. M.; Richard, R. M.; Rohrdanz, M. A.; Steele, R. P.; Sundstrom, E. J.; Woodcock, H. L.; Zimmerman, P. M.; Zuev, D.; Albrecht, B.; Alguire, E.; Austin, B.; Beran, G. J. O.; Bernard, Y. A.; Berquist, E.; Brandhorst, K.; Bravaya, K. B.; Brown, S. T.; Casanova, D.; Chang, C.-M.; Chen, Y.; Chien, S. H.; Closser, K. D.; Crittenden, D. L.; Diedenhofen, M.; DiStasio, R. A.; Do, H.; Dutoi, A. D.; Edgar, R. G.; Fatehi, S.; Fusti-Molnar, L.; Ghysels, A.; Golubeva-Zadorozhnaya, A.; Gomes, J.; Hanson-Heine, M. W. D.; Harbach, P. H. P.; Hauser, A. W.; Hohenstein, E. G.; Holden, Z. C.; Jagau, T.-C.; Ji, H.; Kaduk, B.; Khistyaev, K.; Kim, J.; Kim, J.; King, R. A.; Klunzinger, P.; Kosenkov, D.; Kowalczyk, T.; Krauter, C. M.; Lao, K. U.; Laurent, A. D.; Lawler, K. V.; Levchenko, S. V.; Lin, C. Y.; Liu, F.; Livshits, E.; Lochan, R. C.; Luenser, A.; Manohar, P.; Manzer, S. F.; Mao, S.-P.; Mardirossian, N.; Marenich, A. V.; Maurer, S. A.; Mayhall, N. J.; Neuscamman, E.; Oana, C. M.; Olivares-Amaya, R.; O'Neill, D. P.; Parkhill, J. A.; Perrine, T. M.; Peverati, R.; Prociuk, A.; Rehn, D. R.; Rosta, E.; Russ, N. J.; Sharada, S. M.; Sharma, S.; Small, D. W.; Sodt, A.; Stein, T.; Stück, D.; Su, Y.-C.; Thom, A. J. W.; Tsuchimochi, T.; Vanovschi, V.; Vogt, L.; Vydrov, O.; Wang, T.; Watson, M. A.; Wenzel, J.; White, A.; Williams, C. F.; Yang, J.; Yeganeh, S.; Yost, S. R.; You, Z.-Q.; Zhang, I. Y.; Zhang, X.; Zhao, Y.; Brooks, B. R.; Chan, G. K. L.; Chipman, D. M.; Cramer, C. J.; Goddard, W. A.; Gordon, M. S.; Hehre, W. J.; Klamt, A.; Schaefer, H. F.; Schmidt, M. W.; Sherrill, C. D.; Truhlar, D. G.; Warshel, A.; Xu, X.; Aspuru-Guzik, A.; Baer, R.; Bell, A. T.; Besley, N. A.; Chai, J.-D.; Dreuw, A.; Dunietz, B. D.; Furlani, T. R.; Gwaltney, S. R.; Hsu, C.-P.; Jung, Y.; Kong, J.; Lambrecht, D. S.; Liang, W.; Ochsenfeld, C.; Rassolov, V. A.; Slipchenko, L. V.; Subotnik, J. E.; Van Voorhis, T.; Herbert, J. M.; Krylov, A. I.; Gill, P. M. W.; Head-Gordon, M. Advances in molecular quantum chemistry contained in the Q-Chem 4 program package. *Mol. Phys.* **2015**, *113*, 184−215.
(80) Skrabal, F.; Bangerter, F.; Hamada, K.; Iijima, T. Entropy contribution to an azo dye aggregation in aqueous solution. *Dyes Pigm.* **1987**, *8*, 371−4.
(81) Attwood, D.; Florence, A. T.; Surfactants, in *Physical Pharmacy*; Pharmaceutical Press: London, 2012; Chapter 4.
(82) Redelius, P.; Hansen solubility parameters of asphalt, bitumen, and crude oils, In *Hansen Solubility Parameters: A User's Handbook*, 2nd ed.; CRC Press, Taylor & Francis Group: New York, 2005; Chapter 9.
(83) Acevedo, S.; Castro, A.; Vasquez, E.; Marcano, F.; Ranaudo, M. A. Investigation of the Physical Chemistry Properties of Asphaltenes Using Solubility Parameters of Asphaltenes and their Fractions A1 and A2. *Energy Fuels* **2010**, *24*, 5921−5933.
(84) Mullins, O. C.; Pomerantz, A. E.; Andrews, A. E.; Zuo, J. Y. Asphaltenes explained for the Nonchemist. *Petrophysics* **2015**, *56* (3), 266−275.
(85) Pitonak, M.; Neogrady, P.; Rezac, J.; Jurecka, P.; Urban, M.; Hobza, P. Benzene Dimer: High-Level Wave Function and Density Functional Theory Calculations. *J. Chem. Theory Comput.* **2008**, *4*, 1829−1834.
(86) Pettersson, I.; Liljefors, T.; Lipkowitz, K. B.; Boyd, D. B. Molecular Mechanics Calculated Conformational Energies of Organic Molecules: A Comparison of Force Fields. *Reviews in Computational Chemistry* **2007**, *9*, 167−189.
(87) Ruiz-Morales, Y.; Mullins, O. C. Coarse-Grained Molecular Simulations to Investigate Asphaltenes at the Oil−Water Interface. *Energy Fuels* **2015**, *29* (3), 1597−1609.

DOI: 10.1021/acs.energyfuels.7b01420
Energy Fuels 2017, 31, 9140−9151